Three-Dimensional Analysis of Train-Rail-Bridge Interaction Problems

Article *in* Vehicle System Dynamics · July 2001

DOI: 10.1076/vesd.36.1.1.3567

3 authors:

Yean-Seng Wu
Sinotech Engineering Consultants Corp.
12 PUBLICATIONS **689** CITATIONS
SEE PROFILE

Y.B. Yang
Chongqing University
288 PUBLICATIONS **8,946** CITATIONS
SEE PROFILE

Jong-Dar Yau
Tamkang University
94 PUBLICATIONS **3,284** CITATIONS
SEE PROFILE

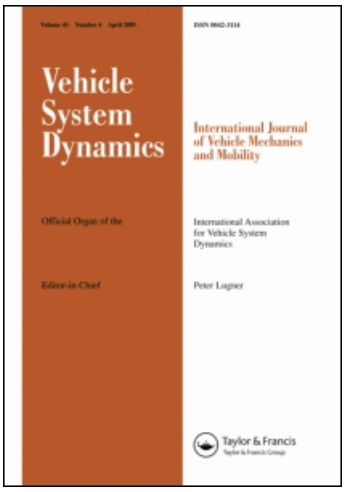

Vehicle System Dynamics
Publication details, including instructions for authors and subscription information:
http://www.informaworld.com/smpp/title~content=t713659010

Three-Dimensional Analysis of Train-Rail-Bridge Interaction Problems

Yean-Seng Wu; Yeong-Bin Yang; Jong-Dar Yau

Online Publication Date: 01 July 2001

To cite this Article Wu, Yean-Seng, Yang, Yeong-Bin and Yau, Jong-Dar(2001)'Three-Dimensional Analysis of Train-Rail-Bridge Interaction Problems',Vehicle System Dynamics,36:1,1 — 35
To link to this Article: DOI: 10.1076/vesd.36.1.1.3567
URL: http://dx.doi.org/10.1076/vesd.36.1.1.3567

Vehicle System Dynamics
2001, Vol. 36, No. 1, pp. 1–35

0042-3114/01/3601-001$16.00

Three-Dimensional Analysis of Train-Rail-Bridge Interaction Problems

YEAN-SENG WU[1], YEONG-BIN YANG[1,3] and JONG-DAR YAU[2]

SUMMARY

A vehicle-rail-bridge interaction (VRBI) model for analysing the 3D dynamic interaction between the moving trains and railway bridge was developed. By the dynamic condensation scheme, three types of vehicle-rail interaction (VRI) elements were derived, by which the vehicle and bridge responses, as well as the wheel / rail contact forces, can be computed. Track irregularity of random nature was taken into account. The results indicate that resonance can occur in both the lateral and torsional vibrations of the bridge, as well as in the vertical vibration. Under the crossing of two face-to-face moving trains, the vertical vibration of the bridge is greatly intensified, while the lateral and torsional responses may be increased or reduced, depending on how the two trains cross each other. Finally, two common indices are used to assess the possibility of derailment for trains passing over the bridge at different speeds.

1. INTRODUCTION

The dynamic response of bridge structures to the train loads has been widely investigated by researchers [1–8]. In most of the previous works, efforts were devoted to study the dynamic interaction between the running trains and railway bridge in the 2D sense concerning primarily the vertical and longitudinal vibrations. For a realistic modelling, however, other dynamic effects need be investigated, e.g., the lateral and rotational or torsional vibrations, the responses induced by two trains in crossing, and so on. In this respect, Chu et al. [9] and Bhatti et al. [10] studied the interaction between the moving trains and steel bridges, along with the impact effects, using 3D bridge and train models. Wakui et al. [11] analysed the response of railway structures

[1]Department of Civil Engineering, National Taiwan University, Taipei, Taiwan, R.O.C.
[2]Department of Architecture and Building Technology, Tamkang University, Taipei, Taiwan, R.O.C.
[3]Corresponding author: Department of Civil Engineering, National Taiwan University, Taipei, Taiwan 10617, R.O.C.

to the passage of trains through 3D modeling. In these studies, however, only some aspects of the dynamic effects of the railway bridge and trains were investigated, while the 3D dynamic interaction effects are not fully explored. Besides, the effect of the track system was either fully ignored or only partially considered. Since the track system is a flexible structure vibrating with the train and bridge, it affects significantly the interaction between the bridge and moving train, especially in the high speed range. For this reason, it is necessary to include the track system in analysis of the train-bridge systems. In the literature, studies on the running behavior and derailment of the trains were carried out by European Rail Research Institute, for which an extract has been given in [12]. In this paper, a 3D vehicle-rail-bridge interaction (VRBI) model that is capable of simulating the 3D dynamic interaction between the moving trains and railway bridges is developed, taking into account the track effects. The dynamic interactions between the moving trains and railway bridge under various conditions are investigated. The possibility of derailment of the train running over the bridge is also evaluated.

2. THREE-DIMENSIONAL MODELS FOR TRAIN, TRACK AND BRIDGE

Figure 1 shows a simply supported railway bridge travelled by a train of speed v. The train is idealized as a series of identical moving vehicles, each

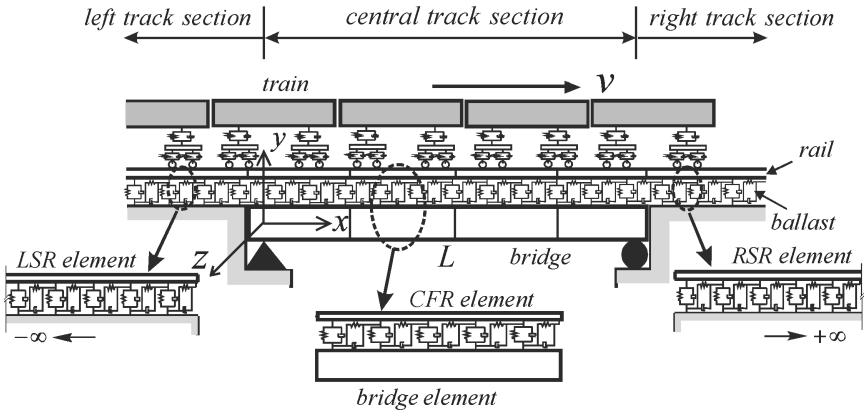

Fig. 1. Simply supported railway bridge travelled by a moving train.

comprising one car body, two bogies and four wheelsets, all assumed to be rigid, as shown in Figure 2(a). The vertical and lateral suspension systems of each vehicle are modelled as linear spring-dashpot units. The bridge is made of a box girder with double tracks, by which the torsional vibration and the effects of two trains crossing on the bridge can be studied. Each of the two tracks is simplified as an infinite and continuous twin rail system lying on a single-layer ballast foundation, as shown in Figure 2(a). The two rails of each track are connected by distributed rigid sleepers. Each rail is treated as a Bernoulli–Euler beam of constant sections. By neglecting the effects of interlock shear, the ballast foundation is represented by uniformly distributed linear spring-dashpot units. Due to the constraint of rigid sleepers, the two rails in the same track have the same longitudinal and lateral displacements. Furthermore, the four wheelsets of each vehicle are supposed to be in touch with the rails at all times (i.e., no jumps occur) and to move with the twin rails in the vertical and lateral directions. Besides, the mass and mass moment of inertia of the sleepers are considered as part of the twin rails. The bridge is idealized as a 3D Bernoulli–Euler beam of constant cross sections. The mass and mass moment of inertia of the ballast layer on the bridge are included as part of those of the bridge. The physical parameters of the vehicle, track and bridge have been shown in Figure 2(a), with their definitions summarized in Tables 1 and 2. In addition, the deviations in geometry of the track, i.e., track irregularities, are taken into account in this study.

3. VEHICLE EQUATIONS AND CONTACT FORCES

All the degrees of freedom (DOFs) permitted of the vehicle body, bogies, and wheelsets are shown in Figure 2(a). The vehicle body has 5 DOFs with respect to its centre of gravity G, i.e., the vertical, lateral, rolling, yawing and pitching DOFs, denoted as $\{d_e\} = \langle v_e\, w_e\, \theta_e\, \phi_e\, \psi_e \rangle^T$. Both the front and rear bogies have 5 DOFs at their centre points, denoted as $\{d_f\} = \langle v_{tf}\, w_{tf}\, \theta_{tf}\, \phi_{tf}\, \psi_{tf} \rangle^T$ and $\{d_r\} = \langle v_{tr}\, w_{tr}\, \theta_{tr}\, \phi_{tr}\, \psi_{tr} \rangle^T$. And each wheelset has 3 DOFs, i.e., the vertical, lateral and rolling DOFs, at the centre of the axle, denoted as $\{d_{wi}\} = \langle v_{wi}\, w_{wi}\, \theta_{wi} \rangle^T$, where $i = 1 \sim 4$. Thus, the *upper part* of the vehicle model, that is, the part not in direct contact with the rails, has a total of 15 DOFs, i.e., $\{d_u\} = \langle \{d_e\} \{d_f\} \{d_r\} \rangle^T$, and the *wheel part* 12 DOFs, i.e., $\{d_w\} = \langle \{d_{w1}\}\ \{d_{w2}\}\ \{d_{w3}\}\ \{d_{w4}\} \rangle^T$. In addition, there exists a total of 8 contact points with the two rails (see also Fig. 2), each of which has a vertical

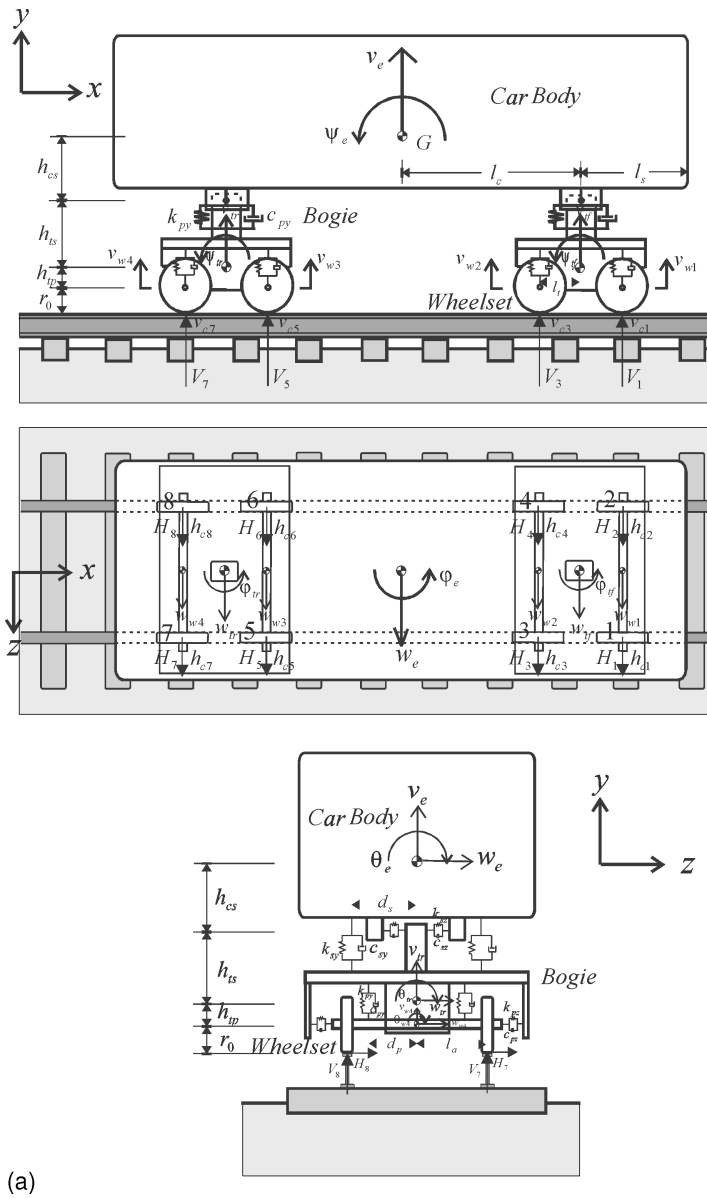

Fig. 2. Vehicle-Bridge model: (a) 3D vehicle.

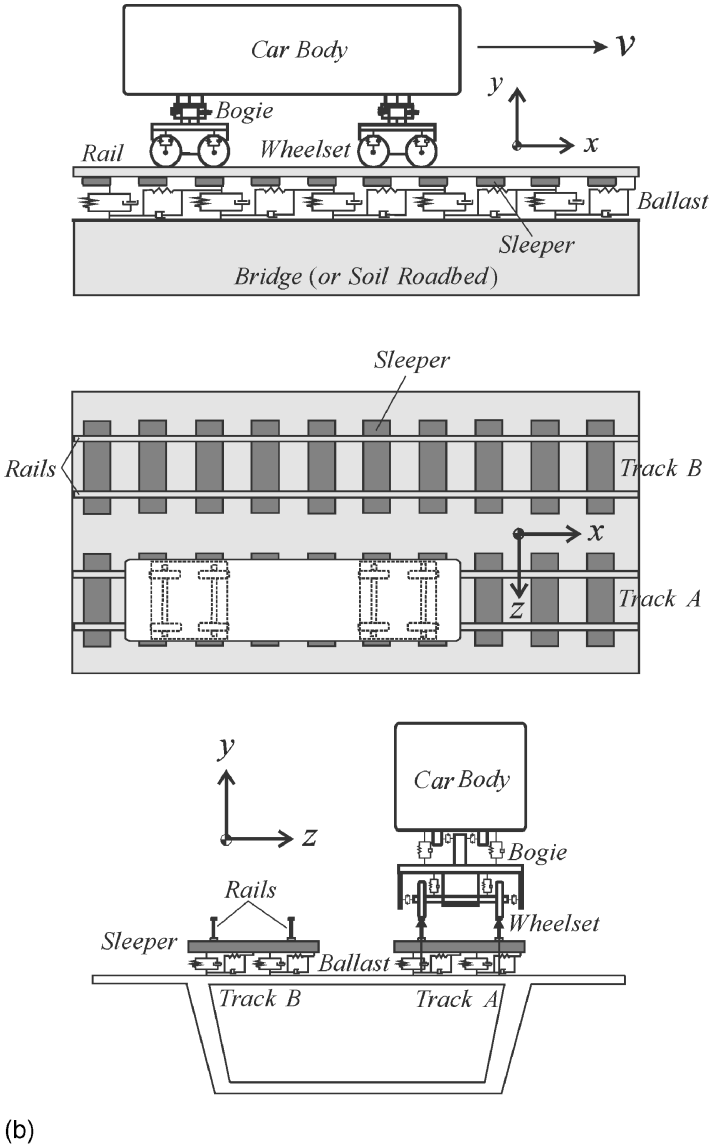

(b)

Fig. 2. Vehicle-bridge model: (b) CFR element.

Table 1. Properties of vehicle model.

Item	Notation	Value*
Mass of car body	M_c	41.75 t
Mass moment of inertia of car body around x axis	I^*_{cx}	23.2 t-m^2
Mass moment of inertia of car body around y axis	I^*_{cy}	2,100 t-m^2
Mass moment of inertia of car body around z axis	I^*_{cz}	2,080 t-m^2
Mass of bogie	M_t	3.04 t
Mass moment of inertia of bogie around x axis	I^*_{tx}	1.58 t-m^2
Mass moment of inertia of bogie around y axis	I^*_{ty}	2.34 t-m^2
Mass moment of inertia of bogie around z axis	I^*_{tz}	3.93 t-m^2
Mass of wheelset	M_w	1.78 t
Mass moment of inertia of wheelset around x axis	I^*_w	1.14 t-m^2
Half of longitudinal distance between center of gravity of car body and of rear bogie	l_c	8.75 m
Half of wheelbase	l_t	1.25 m
Longitudinal distance between center of gravity of bogie and nearest side of car body	l_s	3.75 m
Half of transverse distance between contact points of wheel and rail	l_a	0.75 m
Half of transverse distance between vertical primary suspension systems	d_p	1.00 m
Half of transverse distance between vertical secondary suspension systems	d_s	1.23 m
Vertical distance between center of gravity of car body and lateral secondary suspension system	h_{cs}	0.75 m
Vertical distance between lateral secondary suspension system and center of gravity of bogie	h_{ts}	0.42 m
Vertical distance between center of gravity of bogie and lateral primary suspension system	h_{tp}	0.20 m
Stifffness of vertical primary suspension system	k_{py}	590 kN/m
Damping of vertical primary suspension system	c_{py}	19.6 kN-s/m
Stifffness of lateral primary suspension system	k_{pz}	2,350 kN/m
Damping of lateral primary suspension system	c_{pz}	0 kN/m
Stifffness of vertical secondary suspension system	k_{sy}	265 kN/m
Damping of vertical secondary suspension system	c_{sy}	45.1 kN-s/m
Stifffness of lateral secondary suspension system	k_{sz}	176 kN/m
Damping of lateral secondary suspension system	c_{sz}	39.2 kN-s/m
Nominal radius of wheel	r_0	0.455 m

*1. For SKS series 300 vehicle model
2. Extracted from [11] with some modifications

Table 2. Properties of track and bridge.

Item	Notation	Value*
Track		
Young's modulus	E_t	210 GPa
Poisson's ratio	v_t	0.3
Per-unit-length mass[1]	m_t	0.587 t
Per-unit-length mass moment of inertia about x axis[1]	I_t^*	0.383 t-m^2
Sectional area[2]	A_t	1.5410^{-5} m^2
Flexural moment of inertia about y axis[2]	I_{ty}	1.0310^{-5} m^4
Flexural moment of inertia about z axis[2]	I_{tz}	6.1210^{-5} m^4
Half of gauge of rails	l_a	0.75 m
Half of length of sleeper	l_d	1.3 m
Transverse distance between center lines of track and bridge	l_b	2.35 m
Per-unit-area vertical stiffness of ballast on bridge	K_{bv1}^*	92.3 MN/m^3
Per-unit-area vertical damping of ballast on bridge	C_{bv1}^*	22.6 MN-s/m^3
Per-unit-area lateral stiffness of ballast on bridge	K_{bh1}^*	3.85 MN/m^3
Per-unit-area lateral damping of ballast on bridge	C_{bh1}^*	22.6 MN-s/m^3
Per-unit-area longitudinal stiffness of ballast on bridge	K_{bv1}^*	3.85 MN/m^3
Per-unit-area longitudinal damping of ballast on bridge	C_{bh1}^*	22.6 MN-s/m^3
Per-unit-area vertical stiffness of ballast on approach	K_{bv2}^*	92.3 MN/m^3
Per-unit-area vertical damping of ballast on approach	C_{bv2}^*	22.6 MN-s/m^3
Per-unit-area lateral stiffness of ballast on approach	k_{bv2}^*	3.85 MN/m^3
Per-unit-area lateral damping of ballast on approach	C_{bv2}^*	22.6 MN-s/m^3
Per-unit-area longitudinal stiffness of ballast on approach	k_{bv2}^*	3.85 MN/m^3
Per-unit-area longitudinal damping of ballast on approach	C_{bv2}^*	22.6 MN-s/m3
Sleeper space	d	0.6 m
Bridge		
Young's modulus	E_b	28.25 GPa
Poisson's ratio	v_b	0.2
Per-unit-length mass[3]	m_b	41.74 t
Per-unit-length mass moment of inertia about x axis[3]	I_b^*	495 t-m^2
Sectional area	A_b	7.73 m^2
Torsional moment of inertia about x axis	I_{bx}	15.65 m^4
Flexural moment of inertia about y axis	I_{by}	74.42 m^4
Flexural moment of inertia about z axis	I_{bz}	7.84 m^4
Bridge length	L	30 m
Vertical distance between bridge deck and center of torsion	h	1.2 m

*[1]Including the masses of the rails and sleepers
[2]For two rails
[3]Including the masses of the bridge and ballast

and a lateral DOF. Let v_{ci} and h_{ci} respectively denote the vertical and lateral displacements of the ith contact point. The total *contact-point* DOFs for one vehicle are $\{d_c\} = \langle v_{c1}\, h_{c1}\, v_{c2}\, h_{c2}\, v_{c3}\, h_{c3}\, v_{c4}\, h_{c4}\, v_{c5}\, h_{c5}\, v_{c6}\, h_{c6}\, v_{c7}\, h_{c7}\, v_{c8}\, h_{c8}\rangle^T$. Correspondingly, the *contact forces* are $\{f_c^*\} = \langle V_1\, H_1\, V_2\, H_2\, V_3\ H_3\ V_4\, H_4\, V_5\ H_5\, V_6\ H_6\, V_7\ H_7\ V_8\ H_8\rangle^{\mathrm{T}}$, where V_i and H_i respectively denote the vertical and lateral contact forces of the ith contact point. Because the lateral contact forces acting through the two wheels of each wheelset are the same (i.e., $H_1 = H_2, H_3 = H_4, \ldots$), the contact forces $\{f_c^*\}$ can be rewritten in a *compact form* as $\{f_c\} = \langle V_1\, H_1\, V_2\, V_3\, H_3\, V_4\, V_5\, H_5\, V_6\, V_7\, H_7\, V_8\rangle^T$. In this connection, the vector $\{f_c^*\}$ is referred to as a *complete form*.

In a time-history analysis, one is interested in the behavior of a structure during the time step from t to $t + \Delta t$. The equations of motion for the *vehicle* at time $t + \Delta t$ with partitions for the *upper* (non-contact) and *wheel* (contact) parts can be written as

$$\begin{bmatrix} [m_{uu}] & [m_{uw}] \\ [m_{wu}] & [m_{ww}] \end{bmatrix} \begin{Bmatrix} \{\ddot{d}_u\} \\ \{\ddot{d}_w\} \end{Bmatrix}_{t+\Delta t} + \begin{bmatrix} [c_{uu}] & [c_{uw}] \\ [c_{wu}] & [c_{ww}] \end{bmatrix} \begin{Bmatrix} \{\dot{d}_u\} \\ \{\dot{d}_w\} \end{Bmatrix}_{t+\Delta t}$$
$$+ \begin{bmatrix} [k_{uu}] & [k_{uw}] \\ [k_{wu}] & [k_{ww}] \end{bmatrix} \begin{Bmatrix} \{d_u\} \\ \{d_w\} \end{Bmatrix}_{t+\Delta t} = \begin{Bmatrix} \{f_{ue}\} \\ \{f_{we}\} \end{Bmatrix}_{t+\Delta t} + \begin{bmatrix} [l_u] \\ [l_w] \end{bmatrix} \{f_c\}_{t+\Delta t} \quad (1)$$

where $[m_{uu}]$, $[m_{uw}]$, $[m_{wu}]$ and $[m_{ww}]$ are the partitioned mass matrices, $[c_{uu}]$, $[c_{uw}]$, $[c_{wu}]$ and $[c_{ww}]$ the damping matrices, and $[k_{uu}]$, $[k_{uw}]$, $[k_{wu}]$ and $[k_{ww}]$ the stiffness matrices of the vehicle, with the subscripts u and w denoting the upper and wheel parts, respectively; $\{f_{ue}\}$ and $\{f_{we}\}$ denote the forces acting on the upper and wheel parts; $[l_u]$ and $[l_w]$ the associated transformation matrices; and $\{f_c\}$ denotes the contact forces acting through the four wheelsets. Since the contact forces act only through the wheel part, i.e., the wheelsets, of the vehicle, the transformation matrix for the upper part $[l_u]$ should be set to [0]. The transformation matrix for the wheel part $[l_w]$ is

$$[l_w] = \begin{bmatrix} [l] & & & \\ & [l] & & \\ & & [l] & \\ & & & [l] \end{bmatrix}_{12\times 12} \quad \text{with} \quad [l] = \begin{bmatrix} 1 & 0 & 1 \\ 0 & 2 & 0 \\ -l_a & 2r_0 & l_a \end{bmatrix}_{3\times 3} \quad (2)$$

where l_a denotes half of the axle length of the wheelset and r_0 the nominal radius of the wheel (also see Table 1). All of the other partitioned matrices and vectors involved can be found in [13]. Note that the vehicle is assumed to vibrate from the static equilibrium position.

The wheelset displacements $\{d_w\}$ can be related to the contact-point displacements $\{d_c\}$ of the two rails with surface irregularities by the constraint equation,

$$\{d_w\} = [\Gamma]\{d_c\} + \{R\} \tag{3}$$

Here, $[\Gamma]$ is a constraint matrix and $\{R\}$ a vector used to represent the track irregularities. For the vehicle and rail models considered in this study, the constraint matrix $[\Gamma]$ is

$$[\Gamma] = \begin{bmatrix} [\gamma] & & & \\ & [\gamma] & & \\ & & [\gamma] & \\ & & & [\gamma] \end{bmatrix}_{12\times 16} \quad \text{with} \quad [\gamma] = \begin{bmatrix} \frac{1}{2} & 0 & \frac{1}{2} & 0 \\ 0 & 1 & 0 & 0 \\ -\frac{1}{2l_a} & 0 & \frac{1}{2l_a} & 0 \end{bmatrix}_{3\times 4} \tag{4}$$

and the vector $\{R\}$ represents the rail irregularities at four wheelset positions,

$$\{R\} = \langle \{r_1\} \quad \{r_2\} \quad \{r_3\} \quad \{r_4\} \rangle^T \tag{5}$$

where

$$\{r_i\} = \left\langle \frac{1}{2}[r_{vr}(x_i) + r_{vl}(x_i)] \quad r_h(x_i) \quad \frac{1}{2l_a}[-r_{vr}(x_i) + r_{vl}(x_i)] \right\rangle^T, \quad i = 1 \sim 4 \tag{6}$$

Here, $r_{vr}(x)$ and $r_{vl}(x)$ are the vertical deviations of the two rails, $r_h(x)$ the mean lateral deviations of the two rails, and x_i is the position of the ith wheelset of the vehicle at time $t + \Delta t$.

One key step in analysis of the present interaction problem is to solve for the contact forces $\{f_c\}$ existing between the *moving* (i.e., the vehicle) and the *non-moving* (i.e., the rails) parts. This can be done following the procedure outlined in [14], that is, by solving the upper-part vehicle displacements $\{d_u\}$ from the first row of equation (1) using the Newmark finite difference scheme, and then substituting the displacements $\{d_u\}$ and derivatives into the second

row of equation (1), which will result in the contact forces $\{f_c\}$ at time $t+\Delta t$ as follows:

$$\begin{aligned}\{f_c\}_{t+\Delta t} &= [m_c][\Gamma]\{\ddot{d}_c\}_{t+\Delta t} + [c_c][\Gamma]\{\dot{d}_c\}_{t+\Delta t} + [k_c][\Gamma]\{d_c\}_{t+\Delta t} \\ &\quad + [k_c]\{R\}_{t+\Delta t} + \{p_c\}_{t+\Delta t} + \{q_c\}_t \\ &= [\bar{m}_c]\{\ddot{d}_c\}_{t+\Delta t} + [\bar{c}_c]\{\dot{d}_c\}_{t+\Delta t} \\ &\quad + [\bar{k}_c]\{d_c\}_{t+\Delta t} + \{\bar{p}_c\}_{t+\Delta t} + \{q_c\}_t\end{aligned}$$

where the contact matrices $[m_c]$, $[c_c]$, $[k_c]$ and load vectors $\{p_c\}_{t+\Delta t}$, have been given in [14]. Since the procedure for deriving the contact forces $\{f_c\}$ follows exactly the same lines as that presented as equations (5)–(16) in [14], no attempt will be made herein to recapitulate any of the details in order to save the paper length.

The contact force vector $\{f_c\}$ as presented in equation (7) relates only to the contact-point displacements $\{d_c\}$, which can be augmented through introduction of a transformation matrix $[\lambda]$ to yield the contact forces $\{f_c^*\}$ in *complete form* as

$$\begin{aligned}\{f_c^*\}_{t+\Delta t} &= [\lambda]\{f_c\}_{t+\Delta t} \\ &= [\tilde{m}_c]\{\ddot{d}_c\}_{t+\Delta t} + [\tilde{c}_c]\{\dot{d}_c\}_{t+\Delta t} + [\tilde{k}_c]\{d_c\}_{t+\Delta t} \\ &\quad + \{\tilde{p}_c\}_{t+\Delta t} + \{\tilde{q}_c\}_t\end{aligned} \tag{8}$$

where

$$[\lambda] = \begin{bmatrix} [\delta] & & & \\ & [\delta] & & \\ & & [\delta] & \\ & & & [\delta] \end{bmatrix}_{16\times 12} \quad \text{with} \quad [\delta] = \begin{bmatrix} 1 & 0 & 0 \\ 0 & 1 & 0 \\ 0 & 0 & 1 \\ 0 & 1 & 0 \end{bmatrix}_{4\times 3} \tag{9}$$

and

$$\begin{aligned}&[\tilde{m}_c] = [\lambda][\bar{m}_c], \quad [\tilde{c}_c] = [\lambda][\bar{c}_c], \quad [\tilde{k}_c] = [\lambda][\bar{k}_c] \\ &\{\tilde{p}_c\}_{t+\Delta t} = [\lambda]\{\bar{p}\}_{t+\Delta t}, \quad \{\tilde{q}_c\}_t = [\lambda]\{q\}_t\end{aligned} \tag{10}$$

Through expansion of equation (8), one can obtain the vertical and lateral contact forces for each contact point as

$$V_{i,t+\Delta t} = \tilde{p}_{c(2i-1),\,t+\Delta t} + \tilde{q}_{c(2i-1),t} + \sum_{j=1}^{16} \left(\tilde{m}_{c(2i-1)j}\ \ddot{d}_{cj,t+\Delta t} + \tilde{c}_{c(2i-1)j}\ \dot{d}_{cj,t+\Delta t} + \tilde{k}_{c(2i-1)j}\ d_{cj,t+\Delta t}\right) \quad (11)$$

$$H_{i,t+\Delta t} = \tilde{p}_{c(2i),t+\Delta t} + \tilde{q}_{c(2i),t} + \sum_{j=1}^{16} \left(\tilde{m}_{c(2i)j}\ \ddot{d}_{cj,t+\Delta t} + \tilde{c}_{c(2i)j}\ \dot{d}_{cj,t+\Delta t} + \tilde{k}_{c(2i)j}\ d_{cj,t+\Delta t}\right) \quad (12)$$

where $i = 1 \sim 8$, looping over all the wheels.

4. EQUATIONS FOR TWIN RAIL AND BRIDGE ELEMENTS

Each of the two tracks can be divided into three parts, i.e., the central, left, and right track sections, as shown in Figure 1. In what follows, the track located on the right side of the bridge (when observed along the positive x axis) is referred to as *track A*, and the track on the left side as *track* B. Each of the two tracks of the central track section is modeled as a set of twin rail elements supported by spring-dashpot units and bridge elements. The twin rail elements are of identical length and are collectively referred to as the *central finite rail* (CFR) elements. Moreover, the tracks in the two approaches are modeled as semi-infinite twin rail elements supported by distributed spring-dashpot units, referred collectively to either as the *left semi-infinite rail* (LSR) or *right semi-infinite rail* (*RSR*) elements. Since the two tracks interact with the two sides of the cross section of the bridge, the CFR element for one track is somewhat different from that for the other. However, the LSR or RSR elements for the two tracks A and B are exactly the same for the two side approaches, since they sit on the same stationary road beds.

4.1. CFR Element for Track A

As shown in Figure 2(b), a CFR element and one side of the bridge element are connected by a ballast layer simulated as spring-dashpot units. The CFR and bridge elements are modeled as 3D beam elements of length l. By the virtual

work principle and using interpolation functions for the displacements, the equation of equilibrium for the CFR element can be derived as

$$[m_{tA}]\{\ddot{d}_{tA}\} + [c_{tA}]\{\dot{d}_{tA}\} + [k_{tA}]\{d_{tA}\} = \{f_{tA}\} + [c_{Ab}]\{\dot{d}_b\} + [k_{Ab}]\{d_b\} \quad (13)$$

where $[m_{tA}]$, $[c_{tA}]$ and $[k_{tA}]$ denote the mass, damping and stiffness matrices of the CFR element, with subscript *tA* for *track A*; $\{d_{tA}\}$ and $\{d_b\}$ denote the DOFs of the CFR and bridge elements, respectively; $\{f_{tA}\}$ denotes the external forces; $[c_{Ab}]$ and $[k_{Ab}]$ respectively denote the damping and stiffness matrices induced by the interactions between the bridge and CFR elements.The results for all the matrices in equation (13) can be found in [13].

By replacing the subscript A in each term of equation (13) by B, one can establish the equation of motion for track B. The matrices $[m_{tB}]$, $[c_{tB}]$ and $[k_{tB}]$ for track B are exactly the same as $[m_{tA}]$, $[c_{tA}]$ and $[k_{tA}]$ for track A, while the matrices $[c_{Bb}]$ and $[k_{Bb}]$ are somewhat different from $[c_{Ab}]$ and $[k_{Ab}]$ for track A due to the torsional effect of the bridge element.

4.2. The Bridge Element

The equation of motion for the bridge element can be derived as

$$\begin{aligned}[m_b]\{\ddot{d}_b\} + [c_b]\{\dot{d}_b\} + [k_b]\{d_b\} = \{f_b\} + [c_{bA}]\{\dot{d}_{tA}\} + [k_{bA}]\{d_{tA}\} \\ + [c_{bB}]\{\dot{d}_{tB}\} + [k_{bB}]\{d_{tB}\}\end{aligned} \quad (14)$$

where $\{f_b\}$ denotes the external nodal forces; $[m_b]$, $[c_b]$ and $[k_b]$ denote the mass, damping and stiffness matrices, respectively; $[c_{bA}]$, $[k_{bA}]$ and $[c_{bB}]$, $[k_{bB}]$ represent the track-bridge interaction effects, which are respectively identical to the matrices $[c_{Ab}]$, $[k_{Ab}]$ and $[c_{Bb}]$, $[k_{Bb}]$, namely,

$$[c_{bA}] = [c_{Ab}], \quad [k_{bA}] = [k_{Ab}] \quad [c_{bB}] = [c_{Bb}], \quad [k_{bB}] = [k_{Bb}] \quad (15)$$

4.3. LSR Element for Track A

As shown in Figure 1, the LSR element consists of two semi-infinite beams rigidly connected by bars (sleepers). By the virtual work principle, along with the interpolation functions for semi-infinite field, one can obtain the equation of motion for the LSR element as

$$[m_{sl}]\{\ddot{d}_{tAl}\} + [c_{sl}]\{\dot{d}_{tAl}\} + [k_{sl}]\{d_{tAl}\} = \{f_{tAl}\} \quad (16)$$

where $\{d_{tAl}\}$ denotes the nodal DOFs of the element (6 DOFs) at the start end, $[m_b]$, $[c_b]$ and $[k_b]$ the mass, damping and stiffness matrices, respectively, and $\{f_{tAl}\}$ the nodal external forces. It should be noted that the interpolation functions used in deriving equation (16) were obtained from the static solution to the problem of two rigidly connected beams resting on the Winkler foundation subjected to a unit force or moment at the start end. By replacing the subscripts l in equation (16) by r, one can obtain the equation of motion for the RSR element of track A, with each quantity defined in a similar way.

4.4. LSR Element for Track B

The LSR element for track B is exactly the same as that for track A, except that the DOFs should be replaced by $\{d_{tBl}\}$ and the nodal external forces by $\{f_{tBl}\}$. The equation of motion is

$$[m_{sl}]\{\ddot{d}_{tBl}\} + [c_{sl}]\{\dot{d}_{tBl}\} + [k_{sl}]\{d_{tBl}\} = \{f_{tBl}\} \tag{17}$$

where the matrices $[m_{sl}]$, $[c_{sl}]$ and $[k_{sl}]$ are identical to those of the LSR element for track A. By replacing the subscripts l in equation (17) by r, one obtains the equation of motion for the RSR element of track B, where $[m_{sr}]$, $[c_{sr}]$ and $[k_{sr}]$ are the same as those for track A.

The matrices and vectors involved in the foregoing equations of this section are available in [13]. Note that in a step-by-step time-history analysis, the equations of motion for the CFR, LSR, RSR and bridge elements formulated above should be interpreted as those established for the deformed position of the system at time $t + \Delta t$.

5. VRI ELEMENT CONSIDERING VERTICAL AND LATERAL CONTACT FORCES

Assume that at time $t + \Delta t$, the four wheelsets of a vehicle are acting at the m_1, m_2, m_3 and m_4th twin rail elements of track A or B. The combination of the twin rail elements and the wheelsets acting over them will be grossly referred to as the *vehicle-rail interaction* (VRI) elements. Consider the m_ith element that is acted upon by the vertical and lateral components of the $(2i-1)$th and $(2i)$th contact forces, i.e., $V_{(2i-1),t+\Delta t}$, $H_{(2i-1),t+\Delta t}$, $V_{2i,t+\Delta t}$, and $H_{2i,t+\Delta t}$. The

equation of motion for the m_ith twin rail element of track A at time $t + \Delta t$ can be written as follows:

$$\begin{aligned}[m_{Ai}]\{\ddot{d}_{Ai}\}_{t+\Delta t} + [c_{Ai}]\{\dot{d}_{Ai}\}_{t+\Delta t} + [k_{Ai}]\{d_{Ai}\}_{t+\Delta t} \\ = \{f_{Ai}\}_{t+\Delta t} + \varepsilon_i\left([c_{Ab}]\{\dot{d}_{bi}\} + [k_{Ab}]\{d_{bi}\}\right) - \{f_{Aci}\}_{t+\Delta t}\end{aligned} \tag{18}$$

where $[m_{Ai}] = [m_{tA}]$, $[c_{Ai}] = [c_{tA}]$, $[k_{Ai}] = [k_{tA}]$, $\{d_{Ai}\} = \{d_{tA}\}$ and $\xi_i = 1$ for the case with contact forces acting on the CFR element; $[m_{Ai}] = [m_{sl}]$, $[c_{Ai}] = [c_{sl}]$, $[k_{Ai}] = [k_{sl}]$, $\{d_{Ai}\} = \{d_{tAl}\}$ and $\xi_i = 0$ for the LSR element; $[m_{Ai}] = [m_{sr}]$, $[c_{Ai}] = [c_{sr}]$, $[k_{Ai}] = [k_{sr}]$,$\{d_{Ai}\} = \{d_{tAr}\}$ and $\xi_i = 0$ for the RSR element; and $\{f_{Aci}\}$ denotes the vector of equivalent nodal forces resulting from the action of the $(2i-1)$th and $(2i)$th vertical and lateral contact forces $V_{(2i-1),t+\Delta t}$, $H_{(2i-1),t+\Delta t}$, $V_{2i,t+\Delta t}$, and $H_{2i,t+\Delta t}$

$$\begin{aligned}\{f_{Aci}\}_{t+\Delta t} = \{N_{vi}^R\}V_{(2i-1),t+\Delta t} + \{N_{wi}^R\}H_{(2i-1),t+\Delta t} \\ + \{N_{vi}^L\}V_{(2i),t+\Delta t} + \{N_{wi}^L\}H_{(2i),t+\Delta t}\end{aligned} \tag{19}$$

where $\{N_v^R\}$ and $\{N_w^R\}$ denote the interpolation vectors for the vertical and lateral displacements of the right rail of the m_ith twin rail element, which varies according to whether it is a CFR, RSR or LSR element, to which the contact forces are acting, and $\{N_v^L\}$ and $\{N_w^L\}$ denote similar quantities for the left rail of the m_ith element. The interpolation vectors $\{N_v^R\}$, $\{N_w^R\}$, $\{N_v^L\}$ and $\{N_w^L\}$ for the CFR element are:

$$\begin{aligned}\{N_v^R\} &= \langle 0 \quad N_3 \quad 0 \quad -l_a N_1 \quad 0 \quad N_4 \quad 0 \quad N_5 \quad 0 \quad -l_a N_2 \quad 0 \quad N_6 \rangle^T \\ \{N_w^R\} &= \langle 0 \quad 0 \quad N_3 \quad 0 \quad -N_4 \quad 0 \quad 0 \quad 0 \quad N_5 \quad 0 \quad -N_6 \quad 0 \rangle^T \\ \{N_v^L\} &= \langle 0 \quad N_3 \quad 0 \quad l_a N_1 \quad 0 \quad N_4 \quad 0 \quad N_5 \quad 0 \quad l_a N_2 \quad 0 \quad N_6 \rangle^T \\ \{N_w^L\} &= \{N_w^R\}\end{aligned} \tag{20}$$

and those for the LSR or RSR elements are

$$\begin{aligned}\{N_v^R\} &= \langle 0 \quad N_3 \quad 0 \quad -l_a N_2 \quad 0 \quad N_4 \rangle^T \\ \{N_w^R\} &= \langle 0 \quad 0 \quad N_5 \quad 0 \quad -N_6 \quad 0 \rangle^T \\ \{N_v^L\} &= \langle 0 \quad N_3 \quad 0 \quad l_a N_2 \quad 0 \quad N_4 \rangle^T \\ \{N_w^L\} &= \{N_w^R\}\end{aligned} \tag{21}$$

In equations (20) and (21), the interpolation functions N_1 and N_4 are linear, N_2, N_3, N_5 and N_6 are cubic Hermitian functions [13], which are exactly the interpolation functions used for twin rail and bridge elements in Section 4, and l_a is

half the axle length of the wheelset. The subscript i in $\{N_{vi}^R\}$, $\{N_{wi}^R\}$, $\{N_{vi}^L\}$ and $\{N_{wi}^L\}$ indicates that these vectors are evaluated at the contact position of the ith wheelset, i.e.,

$$\begin{aligned} \{N_{vi}^R\} &= \{N_v^R(\xi_i)\}, \qquad \{N_{wi}^R\} = \{N_w^R(\xi_i)\} \\ \{N_{vi}^L\} &= \{N_v^L(\xi_i)\}, \qquad \{N_{wi}^L\} = \{N_w^L(\xi_i)\} \end{aligned} \tag{22}$$

where ξ is the local coordinate of the position of the ith wheelset on the m_ith element. By use of equations (19), (11) and (12), equation (18) can be rewritten as follows:

$$\begin{aligned} &[m_{Ai}]\{\ddot{d}_{Ai}\}_{t+\Delta t} + [c_{Ai}]\{\dot{d}_{Ai}\}_{t+\Delta t} + [k_{Ai}]\{d_{Ai}\}_{t+\Delta t} \\ &= \{f_{Ai}\}_{t+\Delta t} + \varepsilon_i\left([c_{Ab}]\{\dot{d}_{bi}\}_{t+\Delta t} + [k_{Ab}]\{d_{bi}\}_{t+\Delta t}\right) \\ &\quad - \sum_{j=1}^{4}\left(\left[m_{cij}^*\right]\{\ddot{d}_{rj}\}_{t+\Delta t} + \left[c_{cij}^*\right]\{\dot{d}_{rj}\}_{t+\Delta t} + \left[k_{cij}^*\right]\{d_{rj}\}_{t+\Delta t}\right) \\ &\quad - \{p_{ci}^*\}_{t+\Delta t} - \{q_{ci}^*\}_t \end{aligned} \tag{23}$$

where the asterisked matrices represent the linking action transmitted through the car body by the m_jth element (under the jth wheel load) on the m_ith element (under the ith wheel load) and the interaction between the right and left rails through the four wheelsets,

$$\begin{aligned} \left[m_{cij}^*\right] &= \sum_{k=1}^{4}\left[\{N_i^k\}\left(\sum_{l=1}^{4}\tilde{m}_{c[4(i-1)+k][4(j-1)+l]}\left\langle N_j^l\right\rangle\right)\right] \\ \left[c_{cij}^*\right] &= \sum_{k=1}^{4}\left[\{N_i^k\}\left(\sum_{l=1}^{4}\tilde{c}_{c[4(i-1)+k][4(j-1)+l]}\left\langle N_j^l\right\rangle\right)\right] \\ \left[k_{cij}^*\right] &= \sum_{k=1}^{4}\left[\{N_i^k\}\left(\sum_{l=1}^{4}\tilde{k}_{c[4(i-1),+k][4(j-1)+l]}\left\langle N_j^l\right\rangle\right)\right] \end{aligned} \tag{24a, c}$$

and the equivalent nodal loads are

$$\begin{aligned} \{p_{ci}^*\}_{t+\Delta t} &= \sum_{k=1}^{4}\left(\{N_i^k\}\tilde{p}_{c[4(i-1)+k],t+\Delta t}\right) \\ \{q_{ci}^*\}_t &= \sum_{k=1}^{4}\left(\{N_i^k\}\tilde{q}_{c[4(i-1)+k],t}\right) \end{aligned} \tag{25a, b}$$

where $\{N_\alpha^\beta\}$ is defined as

$$\{N_\alpha^\beta\} = \begin{cases} \{N_{v\alpha}^R\} = \{N_v^R(\xi_\alpha)\}, & \text{for } \beta = 1 \\ \{N_{w\alpha}^R\} = \{N_w^R(\xi_\alpha)\}, & \text{for } \beta = 2 \\ \{N_{v\alpha}^L\} = \{N_v^L(\xi_\alpha)\}, & \text{for } \beta = 3 \\ \{N_{w\alpha}^L\} = \{N_w^L(\xi_\alpha)\}, & \text{for } \beta = 4 \end{cases} \tag{26}$$

The equation of motion as given in (23) is the condensed equation of motion for the VRI element of track A, as all the relevant vehicle DOFs have been eliminated. In a similar way, the condensed equation of motion for the VRI element of track B can be established. All the asterisked matrices and load vectors involved in equations (23) are *time-dependent*, which should be updated at each time step. The condensation process described above should be conducted for all elements directly interacting with the moving vehicles on either or both tracks.

6. SYSTEM EQUATIONS AND STRUCTURAL DAMPING

In this study, the parts of the two rails that are directly acted upon by the wheel loads are modeled by the VRI elements. And the remaining parts not directly under the action of wheel loads are modeled by the ordinary twin rails elements. By assembling all the VRI elements, twin rail elements and bridge elements, the system equations at time $t + \Delta t$ can be established:

$$\begin{aligned} &[M]\{\ddot{D}\}_{t+\Delta t} + [C]\{\dot{D}\}_{t+\Delta t} + [K]\{D\}_{t+\Delta t} \\ &\quad = \{F\}_{t+\Delta t} - \{P_c^*\}_{t+\Delta t} - \{Q_c^*\}_t \end{aligned} \tag{27}$$

where $[M]$, $[C]$ and $[K]$ are the mass, damping and stiffness matrices; $\{D\} = \langle D_A\ D_B\ D_b \rangle^T$ the nodal DOFs of the entire VRBI system, in particular, $\{D_A\}$, $\{D_B\}$and $\{D_b\}$ denote the DOFs associated with track A, track B and the bridge; $\{F\} = \langle F_A\ F_B\ F_b \rangle^T$ denote the corresponding external loads, with $\{F_A\}$, $\{F_B\}$, $\{F_b\}$ indicating the forces pertaining to track A, track B and the bridge; and $\{P_c^*\}_{t+\Delta t}$ and $\{Q_c^*\}_t$ are the equivalent contact forces in global coordinates.

In establishing the system matrices, one first constructs the matrices $[M_0]$, $[C_0]$ and $[K_0]$ for the railway bridge that is free of any vehicle actions, that is,

$$[M_0] = \begin{bmatrix} [M_A] & 0 & 0 \\ 0 & [M_B] & 0 \\ 0 & 0 & [M_b] \end{bmatrix} = \begin{bmatrix} [m_{sl}] + [m_{sr}] + \sum [m_{tA}] & 0 & 0 \\ 0 & [m_{sl}] + [m_{sr}] + \sum [m_{tB}] & 0 \\ 0 & 0 & \sum [m_b] \end{bmatrix} \tag{28a}$$

$$[C_0] = [C_{00}] + [C_{0bt}] = [C_{00}] + \begin{bmatrix} [C_A] & 0 & -[C_{Ab}] \\ 0 & [C_B] & -[C_{Bb}] \\ -[C_{bA}] & -[C_{bB}] & [C_b] \end{bmatrix} = [C_{00}]$$
$$+ \begin{bmatrix} \left(\sum_{i=1}^{4} [c_{sli}]\right) + \left(\sum_{i=1}^{4} [c_{sri}]\right) + \left(\sum \sum_{i=1}^{4} [c_{tAi}]\right) & 0 & -\sum \sum_{i=1}^{6} [c_{Abi}] \\ 0 & \left(\sum_{i=1}^{4} [c_{sli}]\right) + \left(\sum_{i=1}^{4} [c_{sri}]\right) + \left(\sum \sum_{i=1}^{4} [c_{tBi}]\right) & -\sum \sum_{i=1}^{6} [c_{Bbi}] \\ -\sum \sum_{i=1}^{6} [c_{bAi}] & -\sum \sum_{i=1}^{6} [c_{bBi}] & \sum \sum_{i=1}^{9} \left([c_{bi}] + [c'_{bi}]\right) \end{bmatrix} \tag{28b}$$

$$[K_0] = \begin{bmatrix} \left(\sum_{i=1}^{4} [k_{sli}]\right) + \left(\sum_{i=1}^{4} [k_{sri}]\right) + \left(\sum \sum_{i=1}^{4} [k_{tAi}]\right) & 0 & -\sum \sum_{i=1}^{6} [k_{Abi}] \\ 0 & \left(\sum_{i=1}^{4} [k_{sli}]\right) + \left(\sum_{i=1}^{4} [k_{sri}]\right) + \left(\sum \sum_{i=1}^{4} [k_{tBi}]\right) & -\sum \sum_{i=1}^{6} [k_{Bbi}] \\ -\sum \sum_{i=1}^{6} [k_{bAi}] & -\sum \sum_{i=1}^{6} [k_{bBi}] & \sum \sum_{i=1}^{9} \left([k_{bi}] + [k'_{bi}]\right) \end{bmatrix} \tag{28c}$$

and then add to them the interaction effects of vehicles contributed by the VRI elements, as represented by the asterisked terms given in equations (24), to form the system matrices $[M]$, $[C]$ and $[K]$ as follows:

$$[M] = \begin{bmatrix} [M_A] + \left[M_c^*\right] & 0 & 0 \\ 0 & [M_B] + \left[M_c^*\right] & 0 \\ 0 & 0 & [M_b] \end{bmatrix} = \begin{bmatrix} [M_A] + \sum_{k=1}^{n_A} \left(\sum_{i=1}^{4} \sum_{j=1}^{4} \left[m_{cij}^*\right]\right)_k & 0 & 0 \\ 0 & [M_B] + \sum_{k=1}^{n_B} \left(\sum_{i=1}^{4} \sum_{j=1}^{4} \left[m_{cij}^*\right]\right)_k & 0 \\ 0 & 0 & [M_b] \end{bmatrix} \tag{29a}$$

$$
\begin{aligned}
[C] &= [C_{00}] \\
&+ \begin{bmatrix} [C_A] + \left[C_c^*\right] & 0 & -[C_{Ab}] \\ 0 & [C_B] + \left[C_c^*\right] & -[C_{Bb}] \\ -[C_{bA}] & -[C_{bB}] & [C_b] \end{bmatrix} = [C_{00}] \\
&+ \begin{bmatrix} [C_A] + \sum_{k=1}^{n_A} \left(\sum_{i=1}^{4} \sum_{j=1}^{4} \left[c_{cij}^*\right] \right)_k & 0 & -[C_{Ab}] \\ 0 & [C_B] + \sum_{k=1}^{n_B} \left(\sum_{i=1}^{4} \sum_{j=1}^{4} \left[c_{cij}^*\right] \right)_k & -[C_{Bb}] \\ -[C_{bA}] & -[C_{bB}] & [C_b] \end{bmatrix}
\end{aligned} \tag{29b}
$$

$$
\begin{aligned}
[K] &= \begin{bmatrix} [K_A] + \left[K_c^*\right] & 0 & -[K_{Ab}] \\ 0 & [K_B] + \left[K_c^*\right] & -[K_{Bb}] \\ -[K_{bA}] & -[K_{bB}] & [K_b] \end{bmatrix} \\
&= \begin{bmatrix} [K_A] + \sum_{k=1}^{n_A} \left(\sum_{i=1}^{4} \sum_{j=1}^{4} \left[k_{cij}^*\right] \right)_k & 0 & -[K_{Ab}] \\ 0 & [K_B] + \sum_{k=1}^{n_B} \left(\sum_{i=1}^{4} \sum_{j=1}^{4} \left[k_{cij}^*\right] \right)_k & -[K_{Bb}] \\ -[K_{bA}] & -[K_{bB}] & [K_b] \end{bmatrix}
\end{aligned} \tag{29c}
$$

where n_A and n_B denote the number of the vehicles comprising the trains moving on tracks A and B, respectively. Similarly, the equivalent contact forces $\{P_c^*\}_{t+\Delta t}$ and $\{Q_c^*\}_t$ are

$$
\left\{P_c^*\right\}_{t+\Delta t} = \begin{Bmatrix} \sum_{k=1}^{n_A} \left(\sum_{i=1}^{4} \left\{p_{ci}^*\right\}_{t+\Delta t} \right)_k \\ \sum_{k=1}^{n_B} \left(\sum_{i=1}^{4} \left\{p_{ci}^*\right\}_{t+\Delta t} \right)_k \\ 0 \end{Bmatrix}, \quad \left\{Q_c^*\right\}_t = \begin{Bmatrix} \sum_{k=1}^{n_A} \left(\sum_{i=1}^{4} \left\{q_{ci}^*\right\}_t \right)_k \\ \sum_{k=1}^{n_B} \left(\sum_{i=1}^{4} \left\{q_{ci}^*\right\}_t \right)_k \\ 0 \end{Bmatrix} \tag{30a, b}
$$

Note that the subscript k, which indicates the kth vehicle of the train moving on track A (or B), should be looped over from 1 to n_A (or n_B) in order to account for the vehicles effects.

At each time step, it is necessary to check whether a twin rail element becomes a VRI element and vice versa, and to update the entries of the system matrices and vectors, concerning the contribution of the asterisked terms or components in equations (29) and (30), for the DOFs that are directly affected by the vehicle actions, according to variation of the contact positions. One advantage of the present approach is that the total number of DOFs of the VRBI system remains identical to that of the original railway bridge, while the symmetry property of the original system is preserved. In addition, the damping matrix $[C_{00}]$ of the railway bridge in equation (29b) can be determined on the basis of the Rayleigh damping assumption as follows:

$$[C_{00}] = \alpha_0[M_0] + \alpha_1[K_0] \tag{31}$$

where $[M_0]$ and $[K_0]$ are the mass and stiffness matrices of the railway bridge, respectively, and the two coefficients α_0 and α_1 are

$$\alpha_0 = \frac{2\xi\omega_1\omega_2}{\omega_1 + \omega_2}, \quad \alpha_1 = \frac{2\xi}{\omega_1 + \omega_2} \tag{32}$$

where ξ is the damping ratio, ω_1 and ω_2 are the first and second frequencies of vibration of the railway bridge. The Newmark-β method with $\beta = 0.25$ and $\gamma = 0.5$ will be employed for solving the system equations shown in equation (27). The procedure for incremental analysis of the 3D VRBI system is summarized in the flow chart given in Figure 3.

7. SIMULATION OF TRACK IRREGULARITY

Three types of track irregularity, i.e., elevation (vertical profile), alignment and superelevation (cross level), are considered in this study, which can be expressed as stationary processes in space, i.e., as random functions in terms of the longitudinal coordinate x. In railway engineering, the track irregularity is frequently represented by a one-sided power spectral density (PSD)

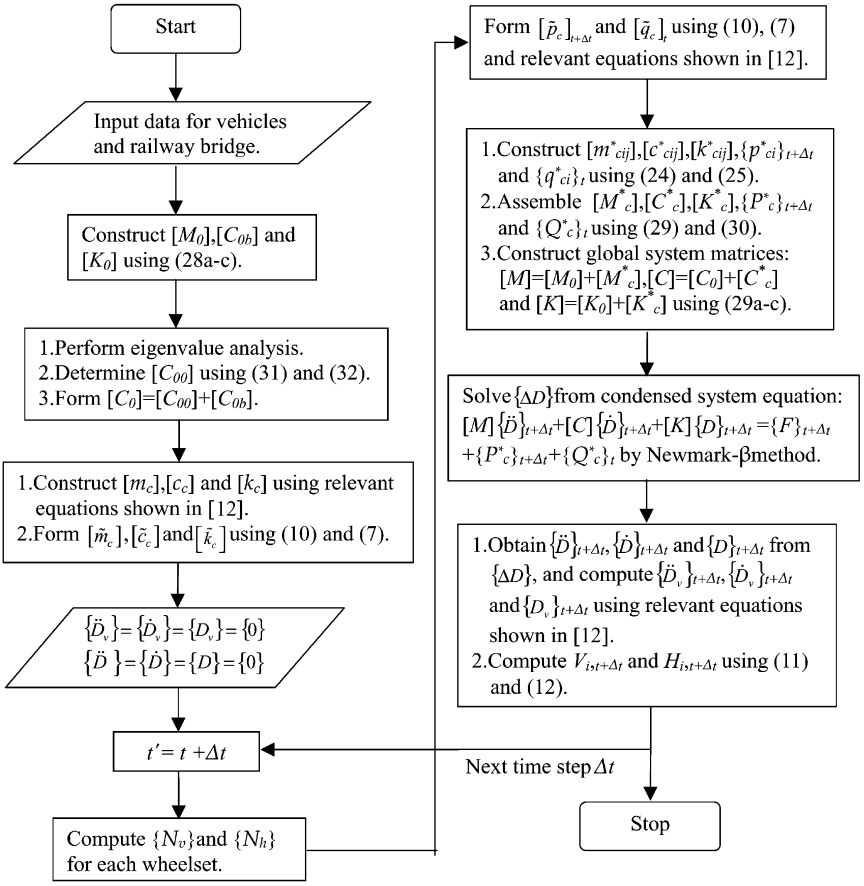

Fig. 3. Procedure for time-history analysis.

function of the track geometry. The PSD functions used in the study for the elevation, alignment and superelevation irregularities are [15]:

$$S_{v,a}(\Omega) = \frac{A_v \Omega_c^2}{\left(\Omega^2 + \Omega_r^2\right)\left(\Omega^2 + \Omega_c^2\right)} \quad \text{for elevation and alignment irregularity} \tag{33a, b}$$

$$S_c(\Omega) = \frac{\left(A_v \Omega_c^2 / l_a\right)\Omega^2}{\left(\Omega^2 + \Omega_r^2\right)\left(\Omega^2 + \Omega_c^2\right)\left(\Omega^2 + \Omega_s^2\right)} \quad \text{for superelevation irregularity}$$

Table 3. Track PSD model parameters.

Quality (FRA Class)	Very Poor (4)	Poor (5)	Moderate (6)
A_v (m)	2.39×10^{-5}	9.35×10^{-6}	1.50×10^{-6}
Ω_s (rad/m)	1.130	0.821	0.438
Ω_r (rad/m)	2.06×10^{-2}	2.06×10^{-2}	2.06×10^{-2}
Ω_c (rad/m)	0.825	0.825	0.825

where $\Omega = 1/L_r$ denotes the spatial frequency (Hz) and L_r the length of the irregularity (m). Table 3 contains the values for the coefficients involved in equation (33), which are equivalent to Classes 4, 5 and 6 of tracks adopted by the Federal Railroad Administration (FRA) [15] with Class 6 indicating the best and Class 4 the worst. By applying the spectral representation method [16], the profiles for the deviation in the elevation, alignment and superelevation, i.e., $r_v(x)$, $r_h(x)$ and $r_c(x)$, of the twin rail system can be established. The results computed for $r_v(x)$, $r_h(x)$ and $r_c(x)$ for FRA track Classes 4, 5 and 6 have been normalized so that their maximum deviations equal the specified values shown in Table 4, which are the maximum tolerated deviations for very poor, poor and moderate tracks according to the standards for high-speed tracks [17]. As a result, the vertical profile and alignment irregularities for the right and left rails can be computed as

$$\begin{aligned} r_{vr}(x) &= r_v(x) - r_c(x) \\ r_{vl}(x) &= r_v(x) + r_c(x) \\ r_{hr}(x) &= r_{hl}(x) = r_h(x) \end{aligned} \tag{34a–c}$$

The profiles of the two rails used for the very poor track (FRA Class 4) were plotted in Figure 4.

Table 4. Maximum tolerable deviations for vertical profile, alignment irregularity and cross level.

Quality (FRA Class)	Very Poor (4)	Poor (5)	Moderate (6)
$r_{v,max}$ (mm)	4.05	3.38	2.70
$r_{h,max}$ (mm)	5.10	4.25	3.40
$r_{c,max}$ (mm)	1.50	1.25	1.00

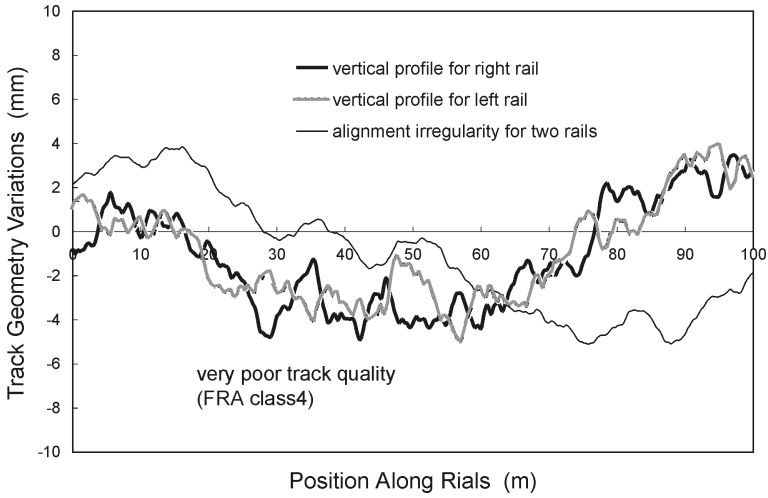

Fig. 4. Irregular vertical and alignment profiles of the two rails (very poor track quality).

8. DYNAMIC CHARACTERISTICS OF 3D TRAIN-RAIL-BRIDGE SYSTEM

8.1. Dynamic Effects Induced by Different Train Speeds

The impact factor I to be used in this study is defined as [7]:

$$I = \frac{R_d(x) - R_s(x)}{R_s(x)} \tag{35}$$

where $R_d(x)$ and $R_s(x)$ denote the maximum dynamic and static responses, respectively, of the bridge at cross section x caused by the moving vehicles. Because of the lack of a lateral static deflection for the bridge, the impact effect for the lateral vibration of the bridge cannot be investigated using the definition (35). Instead, the maximum midspan lateral displacement will be investigated. The non-dimensional speed parameter S adopted here for the train is defined as

$$S = \frac{\pi v}{\omega_1 L} \tag{36}$$

where ω_1 denotes the first natural frequency, L the length of the bridge and v the train speed. For a specific bridge, the speed parameter S is proportional to

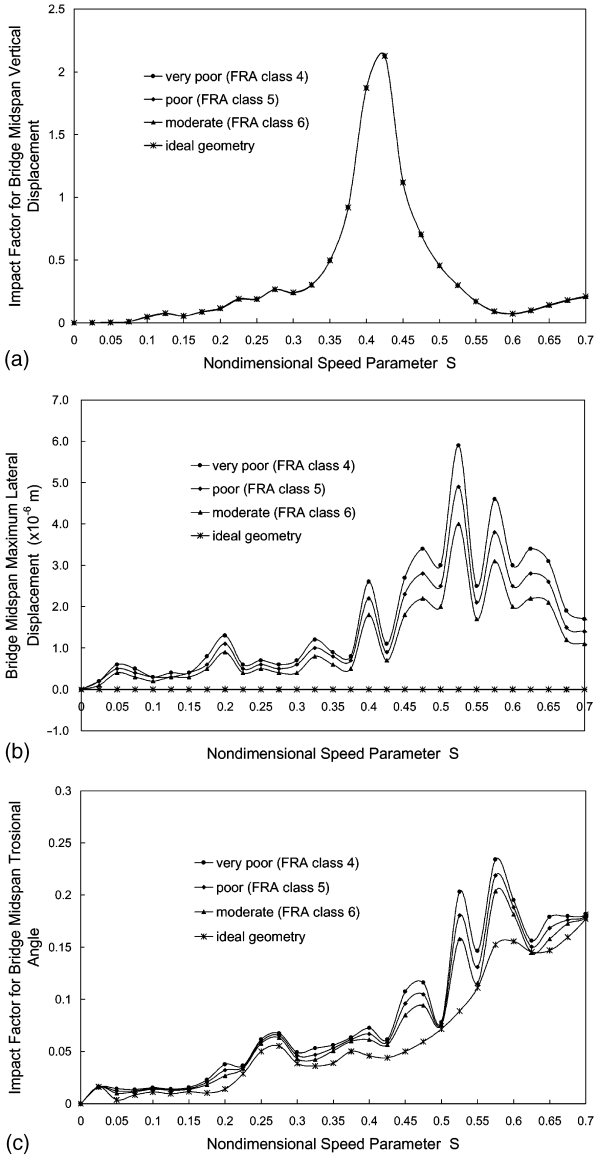

Fig. 5. Impact factor and maximum response for bridge midspan displacements: (a) vertical, (b) lateral, (c) torsional.

Table 5. Asymptotic limits and maximum values of vehicle acceleration.

Vehicle Acceleration	Vertical (m/s^2)	Lateral (m/s^2)	Rolling (rad/s^2)	Yawing (rad/s^2)	Pitching (rad/s^2)
Asymptotic Limit[a]	0.22	0.57	1.22	–	0.04
Maximum Value[b]	0.16	0.53	1.09	0.07	0.03
Tolerable Value[c]	0.98	0.49	–	–	–

a : $v = 0$~600 km / h (very poor track)
b : $v = 0$~360 km / h (very poor track)
c : adopted by Taiwan HSR (UIC = 1 m / s^2, SKS = 1.96 m / s^2, ICE = 0.49 m / s^2 for vertical acceleration)

the train speed. The value of S considered in this study varies from $S = 0$ ($v = 0$ km / hr) to 0.7 ($v = 600$ km / hr). The train is assumed to consist of 15 identical vehicles and is allowed to pass the bridge through track A (see Figure 2(b)). In each running case, the train starts at position $x_0 = -50$ m relative to the bridge and stops at position $x_f = 430$ m. The railway bridge is modeled by 10 elements and the time increment is selected to be $\Delta t = 0.005s$.

The impact responses computed for the midspan of the bridge were plotted in Figure 5 with respect to S for four classes of track quality, namely, the FRA Classes 4, 5, 6 and ideal track geometry. As can be seen, the impact factor for the vertical displacement reaches a peak at $S = 0.425$ ($v = 364$ km / hr), indicating the occurrence of resonance on the bridge. Also, the impact factor is nearly independent of the track quality. The maximum lateral displacement of the bridge reaches its peak at $S = 0.525$ ($v = 450$ km / hr) for all the three FRA classes, but not for the ideal track geometry (which is nearly zero). The reason for this is that the resonance in lateral vibration is caused by the coincidence of any of the driving frequencies of the train with any of the frequencies implied by the track irregularity. Unlike the vertical displacement, the difference in the lateral displacements for the four classes of track quality is generally large.

The impact factor for the midspan torsional angle of the bridge increases with the increase in S, and the difference between the four track classes is rather limited. Also, two local maxima can be observed for the impact factor at $S = 0.525$ and 0.575, which can be attributed to the occurrence of resonance in torsion on the bridge. The maximum impact factors for the midspan vertical and torsional displacements of the bridge are 2.13 and 0.23, respectively, and

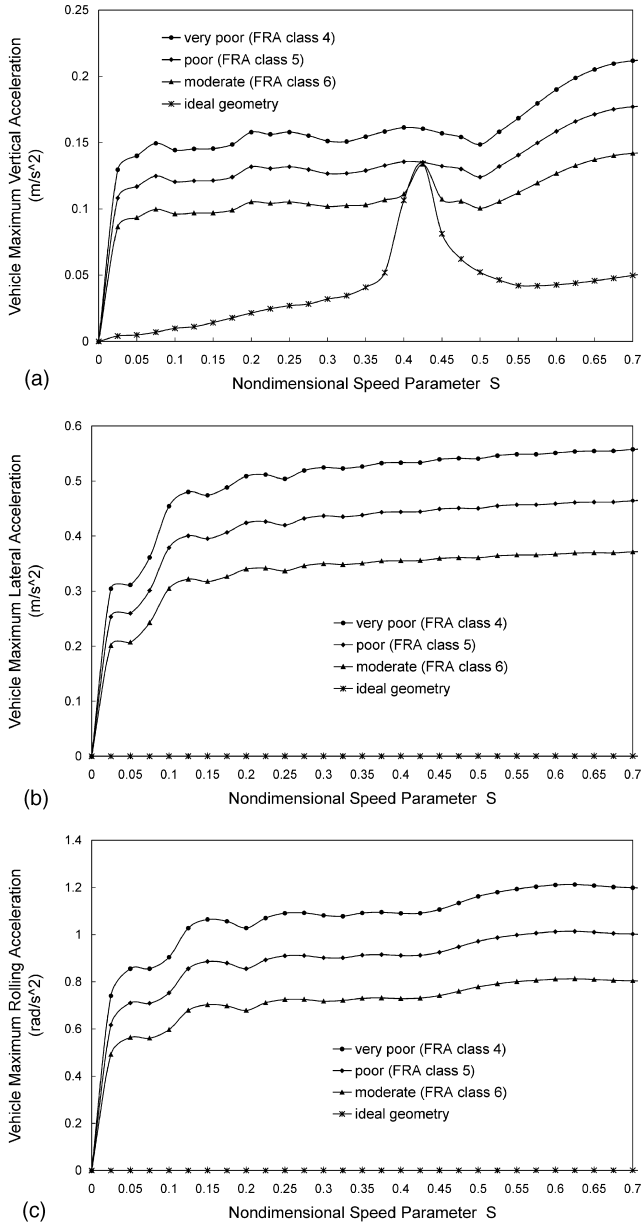

Fig. 6. Maximum vehicle acceleration for different train speeds:
(a) vertical, (b) lateral, (c) rolling, (d) yawing, (e) pitching.

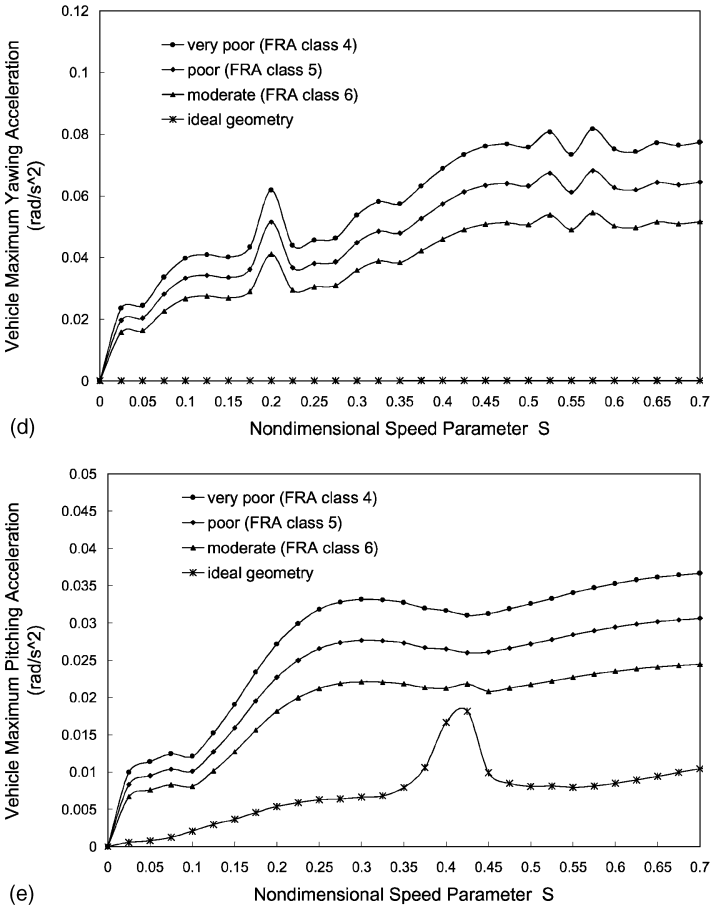

Fig. 6. Continued

the maximum midspan lateral displacement is 0.006 mm. Owing to adoption of the non-dimensional speed parameter S in the analysis, the results reported above for the resonance phenomena may be applied to continuous bridges, if the length L in equation (36) is replaced by the characteristic length of the main span of the continuous bridge [18].

The maximum acceleration of the train with respect to the speed parameter S was plotted in Figure 6 for the four classes of track quality. As can be seen, the maximum acceleration of the train for tracks with irregularities appears to be much larger than that for the ideal track. Moreover, rail irregularities have

much larger difference on the lateral, rolling and yawing response of the train than on the vertical and pitching responses, due to the fact that nearly no lateral, rolling and yawing vibrations are induced on a train as it moves on a smooth straight track. In general, the effect of rail irregularities on the vehicle responses is larger than that of resonance, as indicated by Figures 6(a) and (e). Except for the yawing motion, the maximum accelerations of the train appear to have an asymptotic limit over the whole range of speeds considered. The asymptotic limits have been listed in Table 5, along with the maximum accelerations of the train in the speed range $S < 0.42$ ($V = 360\,\text{km/hr}$) considered by the Taiwan High Speed Railways. As can be seen, the maximum lateral acceleration of the train for the very poor track (FRA Class 4) exceeds the limit of $0.49\,\text{m/s}^2$, but that for the poor track (FRA Class 5) is below the limit, indicating that the track should be maintained regularly to ensure that the maximum deviations are less than those for the poor track, for which the tolerances were given in Table 4.

8.2. Response Induced by Two Trains in Crossing

For a two-way railroad bridge, two trains on two different tracks may cross each other on the bridge with the same or different speeds. The crossing of two trains can result in drastically larger vertical vibrations of the trains and bridge than those by a single train, which is harmful to riding quality of the trains. Three cases will be analysed in this regard: (a) $v_R = 100\,\text{m/s}$, $v_L = 100\,\text{m/s}$, $x_{R0} = 0\,\text{m}$, $x_{Rf} = 430\,\text{m}$, $x_{L0} = 30\,\text{m}$, $x_{Lf} = -400\,\text{m}$, (b) $v_R = 100\,\text{m/s}$, $v_L = 100\,\text{m/s}$, $x_{R0} = 0\,\text{m}$, $x_{Rf} = 430\,\text{m}$, $x_{L0} = 220\,\text{m}$, $x_{Lf} = -400\,\text{m}$, (c) $v_R = 100\,\text{m/s}$, $x_{R0} = 0\,\text{m}$, $x_{Rf} = 430\,\text{m}$ (single train), where v_R, x_{R0} and x_{Rf} respectively denote the speed, starting and stopping positions of the train on track A, and v_L, x_{L0} and x_{Lf} the corresponding quantities for the train on track B. The train on track A is assumed to move along the positive x direction, which will be referred to as train A. The train moving along the negative x direction of track B will be referred to as train B. Each of the two trains consists of 15 identical cars. Case (a) is conceived to study the train and bridge responses caused by two trains crossing each other on the midspan of the bridge ($v = 100\,\text{m/s}$), which will be referred to as *symmetric crossing movement* (in the view point of the bridge). Case (b) is used to study the system responses induced when the mid-portion (i.e., the 8th car) of train A moves to the centre of the bridge, while train B starts to enter the bridge ($v = 100\,\text{m/s}$), which will be referred to as *asymmetric crossing movement*. Case (c) is adopted for comparison only.

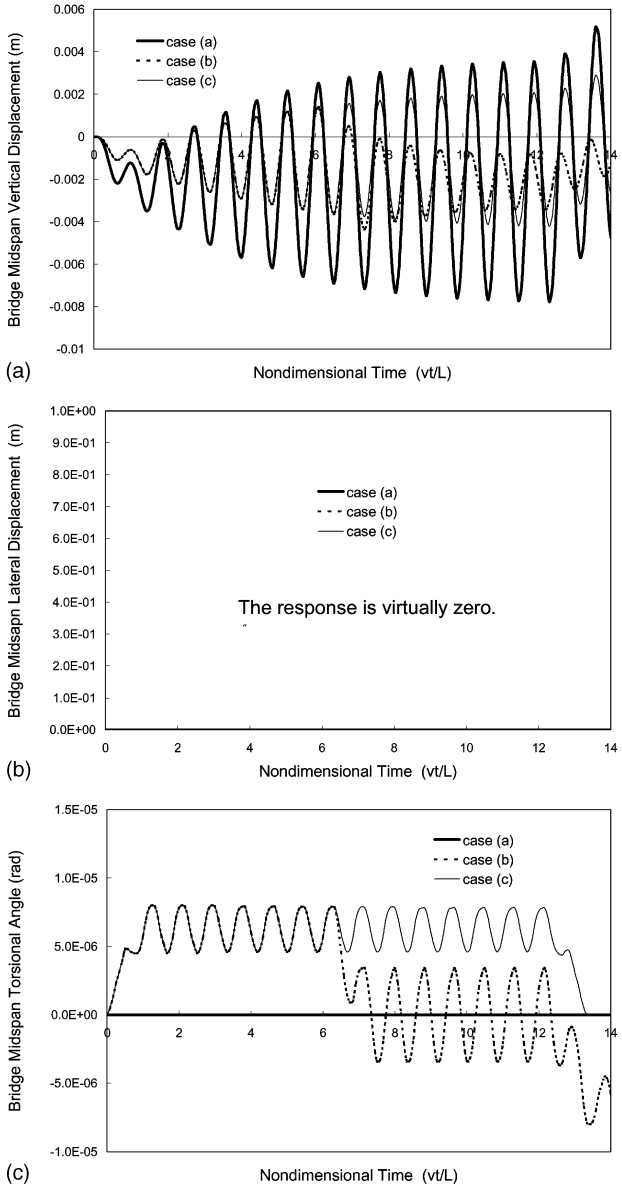

Fig. 7. Bridge responses due to crossing of two trains:
(a) vertical, (b) lateral, (c) torsional.

The results computed for the midpoint of the bridge were shown in Figure 7. As can be seen, the vertical response of the bridge to the symmetric crossing of the two trains (Case (a)) is larger than that to the passage of a single train (Case (c)). The maximum displacements of the bridge are 7.8 and 4.2 mm for Cases

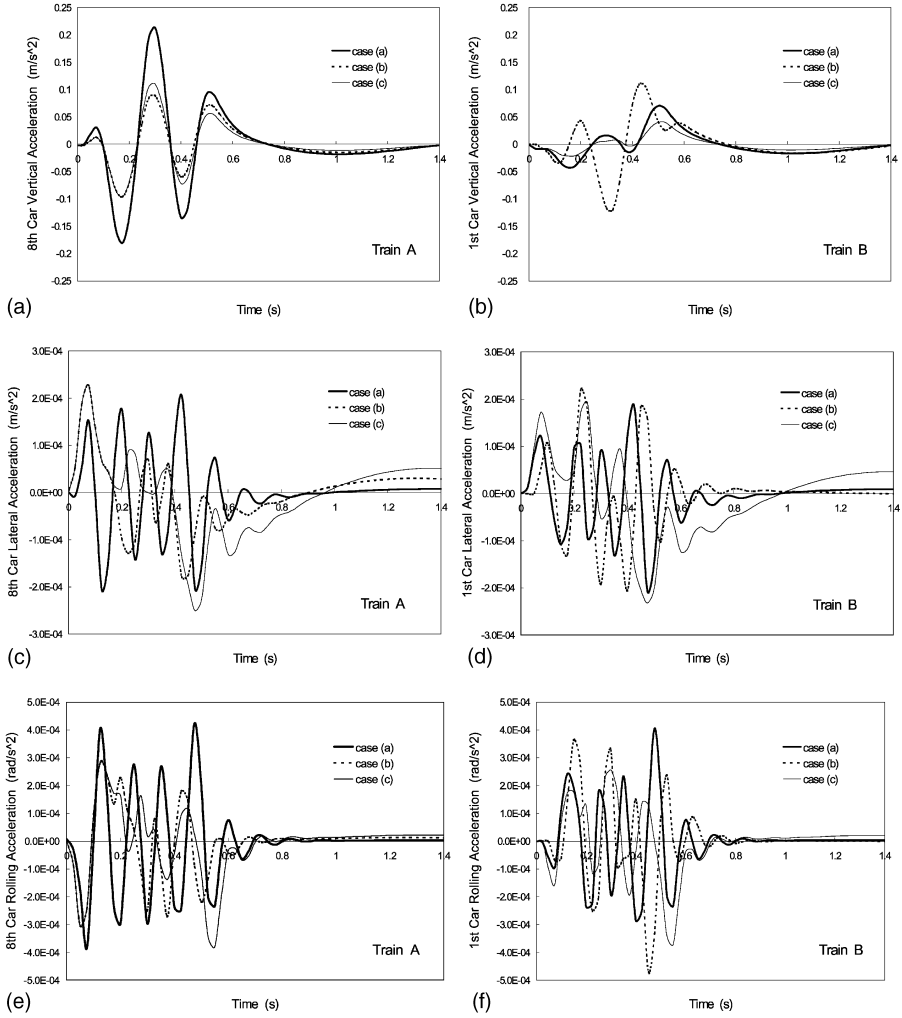

Fig. 8. Vehicle accelerations due to crossing of two trains:
(a–b) vertical, (c–d) lateral, (e–f) rolling, (g–h) yawing, (i–j) pitching

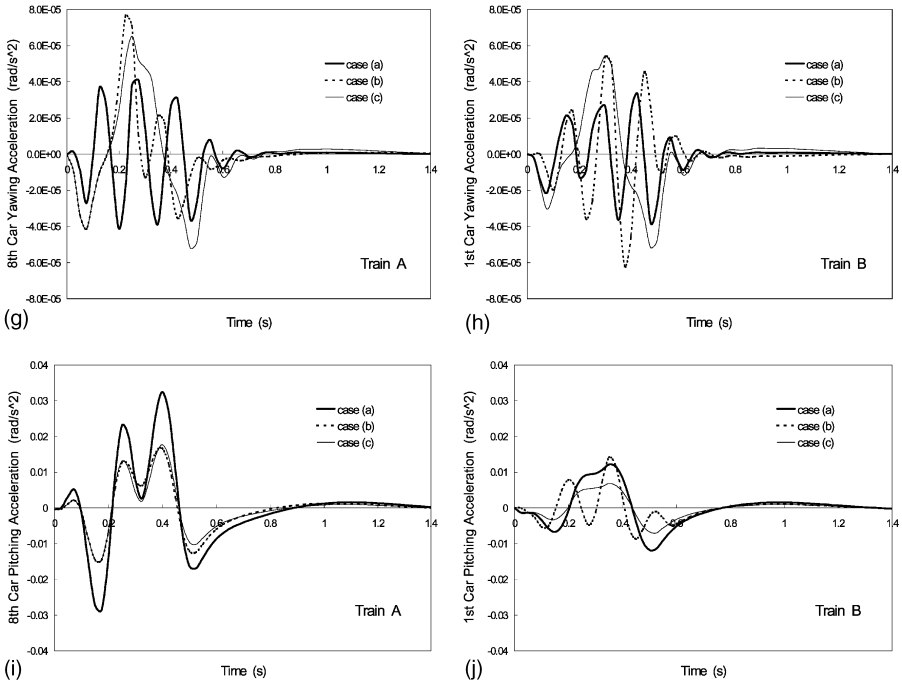

Fig. 8. (Continued)

(a) and (c), respectively. Clearly, the maximum bridge response to the passage of two trains need not be twice large as that for a single train. Of interest is that the vertical response of the bridge for Case (b) becomes smaller than that for Case (c) after train B enters the bridge, i.e., for $vt/L \geq 6.3$. This can be attributed mainly to the cancellation effect of the vehicular loads under asymmetric crossing of the trains. Meanwhile, the lateral displacements of the bridge for the three cases are negligibly small. The midspan torsional response of the bridge for Case (a) is rather small due to cancellation of the torsional moments induced by the two series of loads. The midspan torsional vibrations of the bridge in Cases (b) and (c) are, however, rather large compared with that of Case (a). Furthermore, the torsional vibration in Case (b) changes its equilibrium position from the deformed one by a single train ($\theta_b = 6.5 \times 10^{-6}$ rad) to the undeformed $\theta_b = 0$ rad, and oscillates more drastically than that in Case (c), after the entrance of train B into the bridge ($vt/L \geq 6.3$).

The response of the 8th car of train A and that of the 1st car of train B are selected for investigation, as they are typical of the cars of the two trains crossing on the bridge. From the vehicle responses given in Figure 8(a), one observes that the vertical acceleration of a train under symmetric crossing is larger than that for a single train. Moreover, a train that travels over the bridge first under the condition of asymmetric crossing (e.g., train A in Case (b)) vibrates less severely than it does when travelling alone over the bridge (see Case (c)). On the contrary, the maximum response of a train that travels over the bridge lately under asymmetric crossing (e.g., train B in Case (b)) is larger than the case when it passes alone over the bridge (see Fig. 8(b)). The maximum lateral acceleration of a train induced by symmetric or asymmetric crossing does not differ markedly from that by the passage of a single train (see Figs. 8(c–d)). Similar phenomenon can also be observed for the rolling acceleration of the trains (see Figs. 8(e–f)). However, the maximum response of the yawing acceleration of the train under asymmetric crossing is larger than those by the other two types of train movement (see Figs. 8(g–h)). Least yawing response will be induced on the trains under symmetric crossing. As for the pitching acceleration, the behaviors of the trains are similar to those of the vertical acceleration, namely, trains A and B have the largest responses when the two trains cross each other symmetrically and asymmetrically, respectively, over the bridge (see Figs. 8(i–j)).

8.3. Criteria for Derailment and Safety Assessment of Trains

The running safety of trains has always been of great concern in railway engineering, particularly due to the development of high-speed railways and the need to upgrade existing railways. In this section, two simple criteria for derailment will be employed for assessing the running safety of trains travelling over a bridge.

(i) Wheelset lateral to vertical force ratio (YQ)

This index has been used by many authorities and high-speed rail lines in their specifications, for example, the UIC, ICE, SKS and Mainland China. The YQ ratio is defined as follows: YQ = *Y/Q*, where Y and Q respectively denote the lateral and vertical contact forces acting on a wheelset: $Q = [V_{(2i-1)} + V_{(2i)}] > 0$ and $Y = [H_{(2i-2)} + H_{(2i)}], i = 1, 2, 3$ or 4. If $Q = [V_{(2i-1)} + V(2i)] < 0$, one or two wheels of the ith wheelset will jump, and the train is said to be at a

high degree of risk of derailment. According to the existing specifications, the value of the YQ ratio must not exceed 0.8 to ensure the safety against derailment [19].

(ii) Lateral track force (Y)

A limit is placed on the maximum lateral force exerted by an axle on the track in order to minimize the risk of track panel shift, which has become more important for higher train speeds and the greater use of continuously welded rails. The maximum allowable lateral axle force Y_{lim} (kN) specified by Prud'homme can be given as follows [20]:

$$Y_{lim} = \alpha\left(10 + \frac{Q_s}{3}\right) \quad \text{(kN)} \tag{37}$$

where Q_s is the static axle force (kN) = W, and α is a modification factor; $\alpha = 1.0$ in general and $\alpha = 0.85$ for poorer quality tracks. The maximum allowable lateral axle force is obtained as 55 kN from equation (37) for $W = 135$ kN and $\alpha = 1.0$.

The relation between the maximum values of the above two indices and the train speed (in terms of S) under different track conditions has been plotted in Figures 9(a) and (b). As can be seen, the values of the two indices are all larger for tracks with poorer quality, indicating a higher possibility of train derailment for badly maintained or deteriorating track structures. The YQ index exhibits some local peaks at certain speeds, caused primarily by the lateral train-rail-bridge resonance, as evidenced by Figure 9(b) for the lateral force Y. The difference in the index values for different track qualities is more pronounced at the resonant speeds. The maximum YQ ratio approaches the allowable value of 0.8 at some resonant speeds for the poorest track quality considered (FRA Class 4), implying that the resonance occurring between the train and bridge can greatly aggravate the running instability of the train, particularly for poor track structures.

In general, the index values for higher resonant speeds ($S \geq 0.5$) are larger than those for lower resonant speeds ($S < 0.5$). The train will be at higher risk of derailment when travelling over poor-quality tracks at the resonant speeds. Based on the results obtained for the two criteria, it is concluded that the safety (or stability) of the train passing over the bridge with various speeds for the four track qualities considered is acceptable. However, the train deserves special attention when it moves over tracks of bad qualities. Other relevant results not reported herein are available in [13].

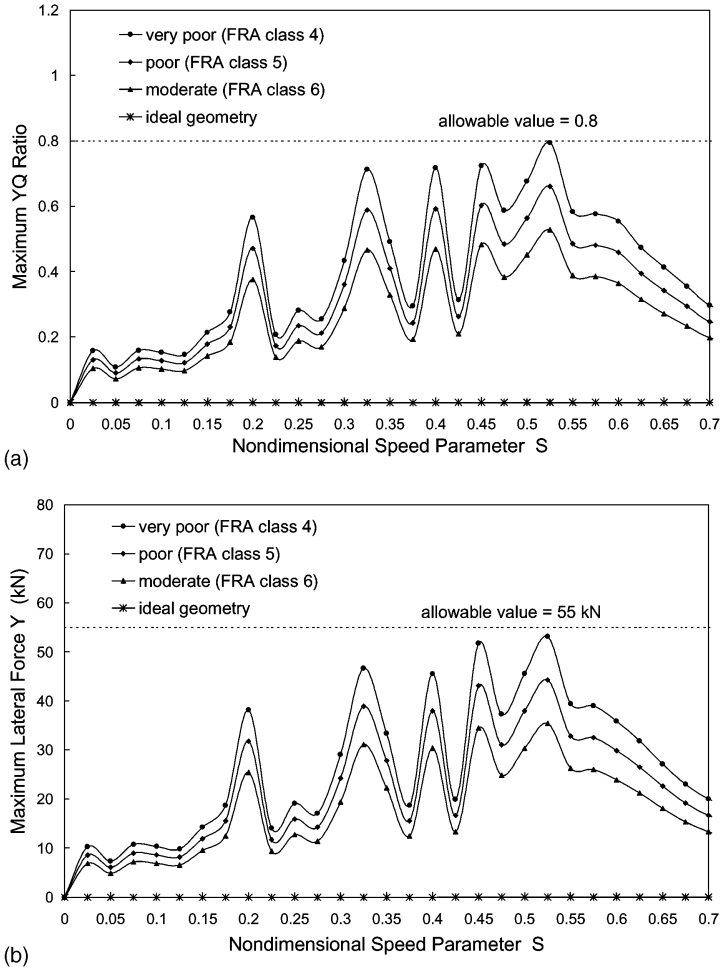

Fig. 9. Maximum index value with relation to train speed:
(a) YQ ratio, (b) lateral contact force Y.

9. CONCLUSIONS

A 3D VRBI model for analysing the train-rail-bridge interactions was established. Such a model allows us to consider the coupling effect between the lateral and rolling vibrations, which may be caused by the difference in elevation of the centres of gravity of the car body, bogie and wheelsets, and the linking action of any two wheels connected by a rigid axle. By taking into

account the constraint imposed by the rigid sleepers on the two rails, the twin rail element enables us to minimize the number of DOFs required in modelling of the track. In addition to the vertical vibration, the lateral and torsional responses of the VRBI system can be obtained simultaneously. Following the dynamic condensation procedure, three types of vehicle-rail interaction (VRI) elements were derived. The equation of motion for the 3D VRBI model was then constructed by assembling the VRI elements, ordinary twin rail elements and bridge elements.

The analysis results indicate that resonance occurs in the lateral and torsional vibrations of the bridge, in addition to the vertical vibration. Also, the presence of track irregularity greatly increases the response of the train and bridge, except for the vertical vibration, for which the impact factor of the bridge is nearly independent of the track quality. Concerning the controllability of running vehicles, track irregularity is an important factor that must be taken into account in design and maintenance of railway bridges. For a two-way railroad bridge, the dynamic effects to be investigated include not only those under the passage of a single train, but also those induced by the crossing of two trains. In general, the vertical vibration of the bridge is more violent under the crossing of two trains, while the lateral and torsional responses may be increased or reduced, depending on the manner of crossing. The vertical and pitching vibrations of the train are evidently exacerbated due to the crossing of two trains. Also, the train tends to oscillate more severe when crossing another train moving at a higher speed.

The possibility of derailment of the train was assessed through the use of two indices. It is found that the train will be at a higher risk of derailment when travelling over a bad-conditioned track, mainly due to the relatively larger lateral forces induced between the wheelset and rails. By comparing the computed indices with the tolerated limits, it is concluded that the train can pass safely through the bridge under the conditions specified in this study for the track irregularity, train model, track and bridge properties, and so on, over a wide range of speeds.

ACKNOWLEDGEMENT

The research reported herein was sponsored by the National Science Council of the Republic of China through Grant. Nos. NSC 89-2211-E-002-122 and 89-2211-E-002-113.

REFERENCES

1. Inglis, C.E.: *A Mathematical Treatise on Vibrations in Railway Bridges*. The University Press, Cambridge, 1934.
2. Frýba, L.: *Vibration of Solids and Structures under Moving Loads*. Noordhoff International Publishing, Groningen, the Netherlands, 1972.
3. Matsuura, A.: A Study of Dynamic Behavior of Bridge Girder for High Speed Railway. *Journal of Structural Mechanics and Earthquake Engineering JSCE* 256 (1976), pp. 35–47. (in Japanese)
4. Aida, T., Green, R. and Hosogi, Y.: Dynamic Behavior of Railway Bridges under Unsprung Masses of a Multi-Vehicle Train. *Journal of Sound and Vibration* 142(2) (1990), pp. 245–260.
5. Frýba, L.: *Dynamics of Railway Bridges*. Thomas Telford Services, London, 1996.
6. Yang, Y.B., Yau, J.D. and Hsu, L.C.: Vibration of Simple Beams due to Trains Moving at High Speeds. *Engineering Structures* 19(11) (1997), pp. 936–944.
7. Yau, J.D., Yang, Y.B. and Kuo, S.R.: Impact Response of High Speed Rail Bridges and Riding Comfort of Rail Cars. *Engineering Structures* 21(9) (1999), pp. 836–844.
8. Li, J.Z. and Su, M.B.: The Resonant Vibration for a Simply Supported Girder Bridge under High-Speed Trains. *Journal of Sound and Vibration* 224(5) (1999), pp. 897–915.
9. Chu, K.H., Garg, V.K. and Dhar, C.L.: Railway-Bridge Impact: Simplified Train and Bridge Model. *Journal of Structural Engineering Division ASCE* 105(9) (1979), pp. 1823–1844.
10. Bhatti, M.H., Garg, V.K. and Chu, K.H.: Dynamic Interaction between Freight Train and Steel Bridge. *Journal of Dynamic Systems, Measurement and Control* 107(1) (1985), pp. 60–66.
11. Wakui, H., Matsumoto, N., Matsuura, A. and Tanabe, M.: Dynamic Interaction Analysis for Railway Vehicles and Structures. *Journal of Structural Mechanics and Earthquake Engineering JSCE* 513(1995), pp. 129–138. (in Japanese)
12. Schupp, G. and Jaschinski, A.: Investigation of Running behavior and Derailment Criteria for Freight Cars by Dynamic Simulation. *COMPRAIL 96, Computers in Railways V.2*, Computational Mechanics Publications, Southampton, UK, 1996, pp. 13–22.
13. Wu, Y.S.: *Dynamic Interactions of Train-Rail-Bridge System under Normal and Seismic Conditions*. Ph.D. thesis, Department of Civil Engineering, National Taiwan University, Taipei, Taiwan, Republic of China, 2000.
14. Yang, Y.B. and Wu, Y.S.: A Versatile Element for Analysing Vehicle-Bridge Interaction Response. *Engineering Structures* 23(3) (2001), pp. 470–483.
15. Fries, R.H. and Coffey, B.M.: A State-Space Approach to the Synthesis of Random Vertical and Crosslevel Rail Irregularities. *Journal of Dynamic Systems, Measurement, and Control ASME* 112(1) (1990), pp. 83–87.
16. Claus, H. and Schiehlen, W.: Modelling and Simulation of Railway Bogie Structural Vibration. *Vehicle System Dynamics Supplement* 28 (1998), pp. 538–552.
17. Esveld, C.: *Modern Railway Track*. Graphics Department of Thyssen Stahl AG, 1989.
18. Yang, Y.B., Liao, S.S. and Lin, B.H.: Impact Formulas for Vehicles Moving over Simple and Continuous Beams. *Journal of Structural Engineering ASCE* 121(11) (1995), pp. 1644–1650.
19. Ma, K.Q and Zhu, J.L.: Seismic Responses Analysis for a System of High-Speed Train and Continuous Rigid-Frame Bridge. *Journal of Shanghai Tiedao University* 19(10) (1998), pp. 29–36. (in Chinese)
20. Elkins, J.A. and Carter, A.: Testing and Analysis Techniques for Safety Assessment of Rail Vehicles: the state-of-the-art. *Vehicle System Dynamics* 22 (1993), pp. 185–208.